Time-encoded spatial routing in a photorefractive crystal

M. Rätsep,* M. Tian,† F. Grelet, and J.-L. Le Gouët

Laboratoire Aimé Cotton, Bâtiment 505, 91405 Orsay Cedex, France

C. Sigel and M.-L. Roblin

Groupe de Physique des Solides, Université Paris VII, Tour 23, 2, Place Jussieu, Paris Cedex 05, France

Received November 20, 1995

The spatial routing of a temporally encoded stream of optical pulses is experimentally demonstrated. The holograms that link the temporally shaped addresses to the deflection directions are engraved in a photorefractive crystal. © 1996 Optical Society of America

After the holography concept was clearly extended from the space to the time domain,[1] it appeared difficult to cope experimentally with the fast flow of short signals that represents the restored image of a temporal hologram. For instance, when such a hologram is engraved in a persistent spectral-hole-burning material embedded in an amorphous material, the retrieved temporal recording can include >1000 subpicosecond pulses, which are sequentially emitted at a rate greater than 1 Tbit/s. Fast optical gating techniques were necessary for sampling the temporal structure of the signal flow,[2,3] but they were not appropriate for simultaneously analyzing a spatial image. Only recently was a fast stream of two-dimensional spatial images successfully stored and retrieved within the frame of space and time holography.[4,5] Meanwhile, the idea also emerged of considering space and time coordinates to be on an equal footing and of designing experiments in which a steady-state spatial image is transformed into a stream of pulses and vice versa.[6–8] This is achieved at the expense of the information content of the data, because one of the spatial dimensions has to be exchanged with the temporal one. This study also aims at combining the spatial and the temporal dimensions in a holographic recording.

Recently[9] a scheme was proposed "to direct temporally structured optical signals originally propagating along a common direction into different and distinct output directions according to the precise temporal waveform encoded onto each signal." A detailed explanation of the process, making use of holograms engraved in frequency-selective materials, is given in Ref. 9. However, it has been suggested that the same routing process could be implemented in materials that possess no intrinsic frequency selectivity. Here we use a nonfrequency-selective photorefractive crystal to demonstrate experimentally the routing of data in temporally encoded spatial directions. Also, we show that, despite the subpicosecond scale of the address code, long-duration pulses can be processed in such a material, if their coherence time is short enough to match the time-scale requirements of the router.

The storage of a temporal structure in a three-dimensional holographic material relies on time–space conversion[6,10] Because a single spatial dimension is used to store the temporal information, two dimensions are left for the engraving of spatial data. Using the same notation as that in Ref. 9, we denote by $E_{1a}(\mathbf{r},t)$ and $E_{2d}(\mathbf{r},t)$ two plane waves that illuminate the material. They counterpropagate in the respective directions $\hat{k}_1$ and $\hat{k}_2$ and are defined as follows:

$$E_\epsilon(\mathbf{r},t) = \mathcal{E}_\epsilon(t - \hat{k}_\epsilon \cdot \mathbf{r}/v)\exp 2i\pi\nu(t - \hat{k}_\epsilon \cdot \mathbf{r}/v)\,, \tag{1}$$

where v is the light's velocity within the active material. These fields are used to program the routing device. A time-encoded address is conveyed by the temporal envelope of the address pulse, E_{1a}. The direction of propagation $\hat{k}_2$ is the spatial information that is conveyed by the direction pulse E_{2d}. The address and the direction are linked together by the interference pattern, which reads as

$$\exp -(2i\pi\nu\hat{K}\cdot\mathbf{r}/v)\int \mathrm{d}t\,\mathcal{E}_{1a}^{*}(t)\mathcal{E}_{2d}(t - \hat{K}\cdot\mathbf{r}/v)\,, \tag{2}$$

where $\hat{K} = \hat{k}_2 - \hat{k}_1$. The interference pattern is engraved in the crystal as a space-dependent variation of the refractive index, which leads to a Bragg grating of vector $2\pi\nu\hat{K}/v$. In the counterpropagating configuration, the grating period is close to $\lambda/2$. Let $\mathcal{E}_{2d}(t)$ be a brief pulse that peaks at $t = 0$. The time integral expresses the sampling analysis of the temporal shape $\mathcal{E}_{1a}(t)$ through the gate $\mathcal{E}_{2d}$. The gate location, $t = \hat{K}\cdot\mathbf{r}/v$, is scanned as a function of the spatial position along direction $\hat{K}$; i.e., the temporal shape $\mathcal{E}_{1a}(t)$ is recorded as the spatial envelope $\mathcal{E}_{1a}(\hat{K}\cdot\mathbf{r}/v)$ of the Bragg grating. An entire address pulse of duration T can be recorded if its spatial extent $vT/2$ is smaller than the length of the engraved interference pattern. In an exact collinear configuration, the sample thickness L limits the address duration to $2L/v$. Storage is still possible when the waves depart from collinear propagation. Then the condition $v[\pi - (\hat{k}_1,\hat{k}_2)]T < 2d$ expresses the trade-off among the maximum object duration T, the collinear propagation angular defect $\pi - (\hat{k}_1,\hat{k}_2)$, and the beam diameter d.

After the programming, the crystal is illuminated by a plane-wave input beam of unit wave vector $\hat{k}_3 = \hat{k}_1$,

0146-9592/96/161292-03$10.00/0

which is diffracted on the Bragg grating in backward direction $\hat{k}_2$. At time t_s the input field is represented by $\mathcal{E}_3(0)$ at position $\mathbf{r} = 0$. The spatial and temporal structure of the deflected beam can be expressed as

$$\exp 2i\pi\nu(t - t_s - \hat{k}_2 \cdot \mathbf{r}/v) \int \mathrm{d}\mathbf{r}' \int \mathrm{d}t' \mathcal{E}_{1a}^*(t' + \hat{K} \cdot \mathbf{r}'/v) \mathcal{E}_{2d}(t') \mathcal{E}_3(t - t_s - \hat{k}_2 \cdot \mathbf{r}/v + \hat{K} \cdot \mathbf{r}'/v). \quad (3)$$

If the direction-programming pulse is brief, the signal-field temporal profile reduces to the cross correlation between the temporal envelopes of the address-programming and the input beams.

Let $\tilde{\mathcal{E}}_\epsilon(f)$ represent the time–frequency Fourier transform of the field $\mathcal{E}_\epsilon(t)$. According to expression (3) the diffracted signal amplitude in direction $\hat{k}_2$ reads as

$$\int \mathrm{d}f \tilde{\mathcal{E}}_{1a}^*(f) \tilde{\mathcal{E}}_{2d}(f) \tilde{\mathcal{E}}_3(f) \times \exp[2i\pi(\nu + f)(t - t_S - \hat{k}_2 \cdot \mathbf{r}/v)]. \quad (4)$$

Phase-only shaping of the pulses in the spectral domain gives rise to sharp correlation peaks. We assume that the envelopes $\tilde{\mathcal{E}}_{1a}(f)$ and $\tilde{\mathcal{E}}_3(f)$ result from the spectral shaping of an initial brief pulse by N-element pseudorandom binary phase codes and that the energy spectral density $|\tilde{\mathcal{E}}_\epsilon(f)|^2$ is uniformly distributed over the storage bandwidth. One code that appears suitable is the so-called maximal length sequence.[11] One can build a set of cross-correlation orthogonal codes by circular permutation of a single sequence. The total diffracted energy, as derived from expression (4), does not depend on the relative spectral phase shifts of $\tilde{\mathcal{E}}_{1a}(f)$ and $\tilde{\mathcal{E}}_3(f)$. But when $\tilde{\mathcal{E}}_{1a}(f)$ and $\tilde{\mathcal{E}}_3(f)$ belong to the same set of orthogonal functions, most of the diffracted energy is concentrated within a correlation peak if and only if $\tilde{\mathcal{E}}_{1a}(f)$ coincides with $\tilde{\mathcal{E}}_3(f)$. Then all encoding spectral phase shifts cancel one another so the correlation peak can be regarded as a replica of the initial input pulse, as it was before spectral shaping.

As explained in Ref. 9, the spatial routing of optical data is carried out as follows. During the programming process, the crystal is successively illuminated by pairs of address and direction pulses. Each address beam propagates in the common direction $\hat{k}_1$ and has a temporal shape (or address) different from that of any other address beam. The ith-direction beam propagates in a direction $\hat{k}_2^{(i)}$ different from that of any of the other programming beams and is temporally shorter than any of the temporal features encoded onto the address beam with which it is paired. By doing this, one creates multiple three-dimensional holograms. Each hologram corresponds to a specific pair of programming pulses. The ith hologram is matched to deflect a correlation peak into the direction $\hat{k}_2^{(i)}$ when an input pulse, incident along $\hat{k}_1$, has the same temporal shape as the ith address beam. In the operational phase, an optical input stream is directed to the programmed material along $\hat{k}_3 = \hat{k}_1$. Whenever a temporal segment of the input data stream matches the ith address, a pulse is deflected in the direction $\hat{k}_2^{(i)}$. Its duration is as short as the inverse storage bandwidth, and it can be detected with a fast discriminator.

Experimental demonstration is achieved in a 6-mm-thick iron-doped $LiNbO_3$ crystal. The maximum length of the address code, as imposed by the crystal thickness, is $2L/v = 100$ ps. All the different beams are split from a single initial beam (see Fig. 1). To build the temporal envelope of the address pulse we follow the spectral encoding procedure developed by Weiner *et al.*[12,13] The spectrum of the pulse can be phase shaped with a liquid-crystal spatial light modulator array that is inserted into a pair of dispersing gratings.[14] However, in this first experiment we simply detect the total energy of the diffracted signals, so we lose the spectral phase information and are able to separate only routing addresses with mutually exclusive spectra. Thus we substitute for the phase modulator a transmission mask composed of five evenly spaced transparent rectangular slits. At the output of the shaper the pulse spectrum, centered at $\lambda = 570$ nm, exhibits a grooved structure, with a 70-GHz-wide bright slice that is repeated every 0.55 THz. A stepping motor translation stage is used to vary the spectral position of the mask, with 0.7-GHz precision. Addresses are orthogonal, provided that the bright spectral slices of the ith address pulse fall onto dark regions of the other address codes.

During the programming the delay between the address and the direction pulses at the center of the crystal is adjusted to zero. The shaped address pulse, with its 70-GHz-wide spectral slices, exhibits a 9-mm-long coherent structure that, owing to the counterpropagation of the direction beam and to the 2.5 refraction index of $LiNbO_3$, shrinks to a 1.8-mm-long hologram. Two holograms are engraved in the crystal. The angle between $\hat{k}_2^{(1)}$ and $\hat{k}_2^{(2)}$ is 100 mrad. With a beam diameter of 250 μm on the crystal, this angle is small enough to allow all the temporal codes to be stored.

The bright spectral slices of address code 2 are set halfway between those of code 1. This configuration is illustrated in Fig. 2, in which the corresponding tem-

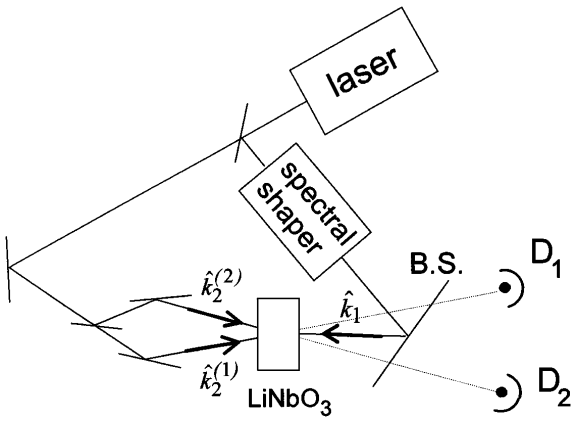

Fig. 1. Diagram of the experimental setup: Two holograms are sequentially recorded. Then beams $\hat{k}_2^{(1)}$ and $\hat{k}_2^{(2)}$ are blocked and the diffracted signals are simultaneously detected on photodiodes D_1 and D_2 through the beam splitter (B.S.).

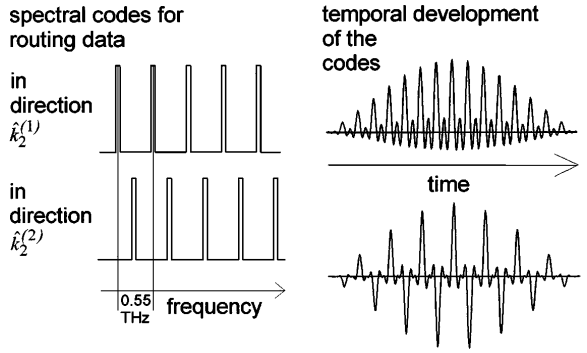

Fig. 2. Spectral slits used to encode the address beams. One obtains the corresponding temporal developments by Fourier transform of the spectral shapes. The code 1 center is set to coincide with that of the laser spectrum.

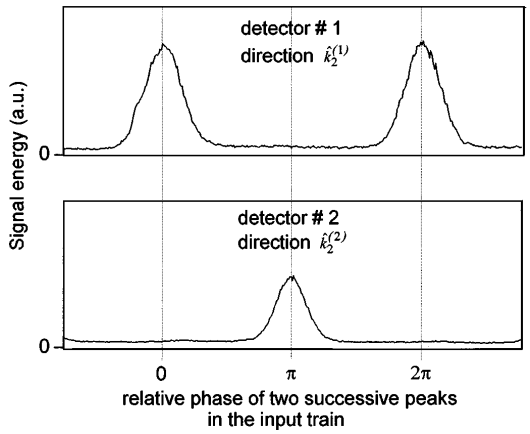

Fig. 3. Experimental data: A spectrally encoded pulse stream is directed to the programmed optical processor along $\hat{k}_1$. Diffracted energy is simultaneously detected in directions $\hat{k}_2^{(1)}$ and $\hat{k}_2^{(2)}$ as a function of the spectral position of the shaping mask. The position scan is equivalent to the scan of the relative phase of two successive peaks within the temporal profile of the input pulse. The detector zero level is represented by 0 on the vertical axis.

poral profiles are also shown. With an appropriate choice of the origin of energy, there is no phase shift between the peaks that comprise the time-domain representation of code 1, and there is a π phase shift between two successive peaks in the train that describes code 2. After the recording, the direction beams are blocked. A spectrally shaped beam is directed to the engraved hologram along $\hat{k}_1$. The diffracted energy is simultaneously detected on two avalanche photodiodes in directions $\hat{k}_2^{(1)}$ and $\hat{k}_2^{(2)}$. The experimental data are displayed in Fig. 3 as a function of the spectral position of the shaping mask. This spectral scan is regarded as the scan of the phase shift between two successive peaks in the temporal development of the input pulse. The background, which is observed outside the matched filtering regions, is caused mainly by the scattering of the input beam in the beam splitter through which the diffracted light is detected (see Fig. 1). The measured cross talk between the routing addresses is smaller than 10^{-2}. The matched temporal shapes are diffracted onto the engraved gratings with an efficiency of $\sim 10^{-5}$. It can be observed that the full width at half-maximum of the recorded profiles (Fig. 3) is larger than expected. As expressed in terms of phase shift, it amounts to $\sim 1/6$ of 2π, instead of $1/8$ of 2π, which is the ratio of the spectral slit size to their period. To focus the spectrally shaped beam upon the crystal we were obliged to depart from the exact position of imaging of the mask upon the sample. As explained in Ref. 15, this results in the observed broadening of the recorded profiles.

In the above discussion, we considered temporal profiles that exhibit subpicosecond peaks. Their three-dimensional hologram recording results from their sampled analysis by use of an optical gating pulse that has to be shorter than the profiles. However, a chaotic nanosecond source (pulse width $\cong 7$ ns) has been used instead of a femtosecond laser in this experiment.

To take full advantage of the time-encoding procedure, one has to detect the correlation peak that is deflected in the matched direction. Interferometric cross correlators similar to the one used in Ref. 14 could operate as discriminators in each routing direction.

*Permanent address, Institute of Physics, Estonian Academy of Sciences, EE2400 Tartu, Estonia.
†Permanent address, Changchun Institute of Physics, Academia Sinica, Changchun 130021, China.

References

1. T. W. Mossberg, Opt. Lett. **7,** 77 (1982).
2. A. Rebane, J. Aaviskoo, and J. Kuhl, Appl. Phys. Lett. **54,** 93 (1989).
3. A. Débarre, J.-C. Keller, J.-L. Le Gouët, P. Tchénio, and J.-P. Galaup, J. Opt. Soc. Am. B **8,** 2529 (1991).
4. K. B. Hill, K. G. Purchase, and D. J. Brady, Opt. Lett. **20,** 1201 (1995).
5. A. Rebane, "Storage and processing of femtosecond optical signals," presented at the Optical Society of America Annual Meeting, Portland, Ore., September 1995.
6. Yu. T. Mazurenko, Opt. Spektrosk. **57,** 569 (1984); Appl. Phys. B **50,** 101 (1990).
7. K. Ema, M. Kuwata-Gonokami, and F. Shimizu, Appl. Phys. Lett. **59,** 2799 (1991).
8. A. M. Weiner, D. E. Leaird, D. H. Reitze, and E. Gi Paek, IEEE J. Quantum Electron. **28,** 11 551 (1992).
9. W. R. Babbitt and T. W. Mossberg, Opt. Lett. **20,** 910 (1995).
10. C. Joubert, M.-L. Roblin, and R. Grousson, Appl. Opt. **28,** 4604 (1989).
11. A. M. Weiner, J. P. Heritage, and J. A. Salehi, Opt. Lett. **13,** 300 (1988).
12. A. M. Weiner, J. P. Heritage, and E. M. Kirschner, J. Opt. Soc. Am. B **5,** 1563 (1988).
13. M. M. Wefers and K. A. Nelson, J. Opt. Soc. Am. B **12,** 1343 (1995).
14. M. Rätsep, M. Tian, I. Lorgeré, F. Grelet, and J.-L. Le Gouët, Opt. Lett. **21,** 83 (1996).
15. I. Lorgeré, M. Rätsep, J.-L. Le Gouët, F. Grelet, M. Tian, A. Débarre, and P. Tchénio, J. Phys. B **28,** 565 (1995).